Fissural volcanism, polygenetic volcanic fields, and crustal thickness in the Payen Volcanic Complex on the central Andes foreland (Mendoza, Argentina)

F. Mazzarini and A. Fornaciai

Istituto Nazionale di Geofisica e Vulcanologia, Via della Faggiola 32, I-56126 Pisa, Italy (mazzarini@pi.ingv.it)

A. Bistacchi

Dipartimento di Scienze Geologiche e Geotecnologie, Università degli Studi di Milano–Bicocca, Piazza della Scienza 4, I-20126 Milan, Italy

F. A. Pasquarè

Dipartimento di Scienze Chimiche ed Ambientali, Università degli Studi dell'Insubria, Via Valleggio 11, I-22100 Como, Italy

[1] Shield volcanoes, caldera-bearing stratovolcanoes, and monogenetic cones compose the large fissural Payen Volcanic Complex, located in the Andes foreland between latitude 35°S and 38°S. The late Pliocene-Pleistocene and recent volcanic activity along E-W trending eruptive fissures produced basaltic lavas showing a within-plate geochemical signature. The spatial distribution of fractures and monogenetic vents is characterized by self-similar clustering with well defined power law distributions. Vents have average spacing of 1.27 km and fractal exponent $D = 1.33$ defined in the range 0.7–49.3 km. The fractal exponent of fractures is 1.62 in the range 1.5–48.1 km. The upper cutoffs of fractures and vent fractal distributions (about 48–49 km) scale to the crustal thickness in the area, as derived from geophysical data. This analysis determines fractured media (crust) thickness associated with basaltic retroarc eruptions. We propose that the Payen Volcanic Complex was and is still active under an E-W crustal shortening regime.

1. Introduction

[2] Volcanism mainly concentrates at plate margins and is quite common in extensional settings, whereas in compressional ones it is assumed by some authors that magma cannot easily reach the surface [e.g., *Watanabe et al.*, 1999]. Recent investigations focused the attention on the emplacement

of shallow crustal-level intrusions [*Musumeci et al.*, 2005] and volcanism [*Tibaldi*, 2005; *Galland et al.*, 2007a, 2007b] during crustal shortening. Several examples of volcanoes growing in contractional tectonic settings have been identified in the Andes: e.g., the El Reventador and Guaga Pichincha volcanoes in Ecuador [*Tibaldi*, 2005; *Legrand et al.*, 2002] and the Taapaca and Socompa volcanoes in Chile [*Clavero et al.*, 2004; *van Wyk de Vries et al.*, 2001]. In the Andes Foreland Belt at 37°S latitude, field evidence, along with radiometric ^{39}Ar-^{40}Ar ages, shows that the Quaternary basaltic Tromen volcano (Argentina) developed above active thrust systems coeval with regional crustal shortening [*Galland et al.*, 2007a, and references therein]. Alternatively, *Folguera et al.* [2008], on the basis of the analysis of seismic data and field observations, associated the Tromen volcanism with crustal collapse and extension during the Quaternary.

[3] A large Pleistocene-recent composite volcanic field, the Payen Volcanic Complex [*Inbar and Risso*, 2001; *Pasquarè et al.*, 2008] developed just 100 km northeast of Tromen Volcano, above the Neuquén Basin in the Mendoza province of Argentina [*Cobbold et al.*, 1999]. The Payen Volcanic Complex comprises basaltic shield volcanoes, basaltic scoria cones, scoria and spatter cones, and trachyandesitic stratovolcanoes aligned along an E-W trending eruptive fissure, several tens of kilometers long [*Inbar and Risso*, 2001; *Pasquarè et al.*, 2005; *Bertotto et al.*, 2006; *Risso et al.*, 2008; *Pasquarè et al.*, 2008]. In this paper the spatial distribution of monogenetic vents and of the fracture network in the Payen Volcanic Complex are described and then discussed in the light of a possible relationship with the crustal thickness in the sector of the Andes foreland between latitude 35°S and 38°S.

2. Geodynamic and Geologic Framework and Crustal Structure

[4] The tectonic setting of the studied area is dominated by the convergence between the Nazca and South America plates (Figure 1) at a mean rate of 80 mm a^{-1}, averaged at this latitude over the last 3 Ma [*Somoza*, 1998], or 66 mm a^{-1} with an azimuth of 79.5° determined on the basis of GPS modeling [*Kendrick et al.*, 2003]. At the latitude of 38°S, the Nazca-South America convergence is accommodated in intraarc and back-arc zones by strain partitioning associated with transpression in the intraarc [*Folguera et al.*, 2004; *Rosenau et al.*,

2006]. Analyses of GPS-derived velocity field highlight that the deformation is localized in the back-arc zone in southern Andes (26°–36°S), suggesting a locking of the Nazca oceanic boundary and the possible occurrence of an "Andes" microplate colliding with the back arc [*Brooks et al.*, 2003]. Present-day crustal deformation rates in the central and southern sections of the Andes, derived by the analysis of GPS data, reveal an E-W trending contraction in the order of 10 mm a^{-1} in the Andes retro-arc at 36°S–37°S latitude [*Klotz et al.*, 2001; *Wang et al.*, 2007]. In Miocene and Holocene times, mixed contractional and extensional tectonic regimes affected the eastern slope of the Andes at 36°–39°S latitude [*Folguera et al.*, 2006]. This complex geodynamic scenario is explained by post-Miocene changes in the subduction zone geometries that affected different segments of the Andes. Notably, north of 38°S latitude, the extension is limited to the period between 5 and 3 Ma [*Folguera et al.*, 2006].

[5] The Payen Volcanic Complex developed in the northern sector of the back-arc Neuquén Basin, north of 38°S latitude (Figure 1), and belongs to the volcanic province of Payenia [*Polansky*, 1954; *Ramos*, 1999; *Inbar and Risso*, 2001; *Pasquarè et al.*, 2005; *Bertotto et al.*, 2006; *Ramos and Kay*, 2006]. Its western sector reaches the Andean margin near the junction between the N-S trending Malargue Fold and Thrust Belt, in the north, and the Agrio Fold Belt, in the south [*Cobbold et al.*, 1999; *Cobbold and Rossello*, 2003; *Guzman et al.*, 2007]. Analysis of the active stress field in the crust of the Neuquén Basin has been performed by studying borehole breakout orientations from numerous wells [*Guzman et al.*, 2007]. In the basin as a whole, the maximum horizontal stress is directed nearly E-W (91°), but there is a small difference in azimuth between data north of Rio Colorado (100°) and those south of Rio Colorado (82°) [*Guzman et al.*, 2007]. In the Payen Volcanic Complex area, the orientation of the maximum horizontal stress, derived from borehole breakouts [*Guzman et al.*, 2007], ranges from 70° to 127° with an average, E-W orientation (Figure 1). E-W monogenetic vent alignments have also been recognized in the northern portion of the volcanic complex [*Risso et al.*, 2008]. Moreover, in the Tromen volcano area, further south of the Payen Volcanic Complex, late Pliocene-Pleistocene dykes trend E-W [*Galland et al.*, 2007a]. The Ar^{39}–Ar^{40} plateau ages of the Tromen volcanic products in the work of *Galland et al.* [2007a] depict a complex evolution of the volcano starting about at 2.3 Ma, characterized by
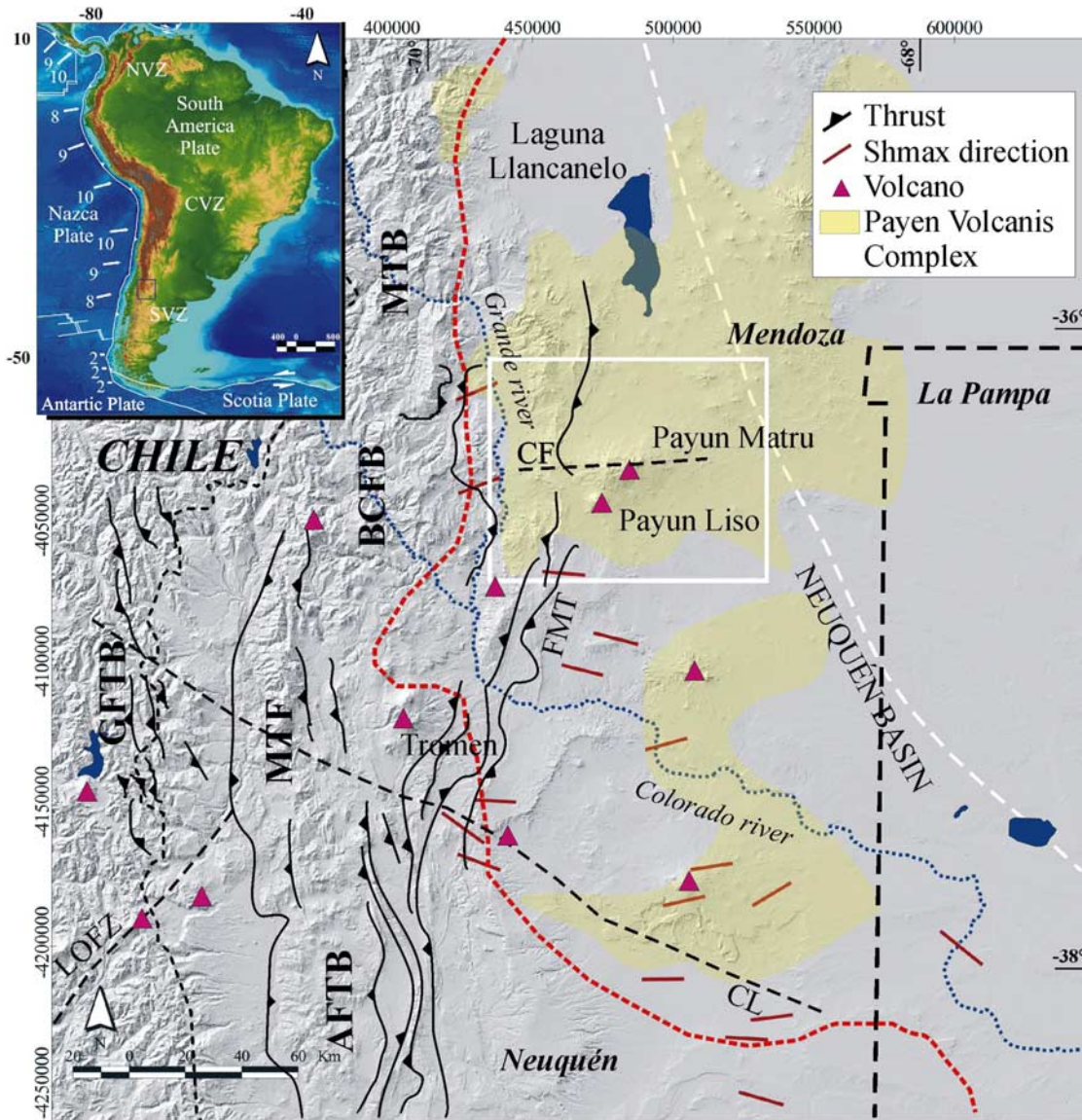
Figure 1. Geology framework of the Andean Foreland between 35°S and 39°S latitude. The Shaded DEM, illuminated from the NW, is derived from SRTM (courtesy of the University of Maryland Global Land Cover Facility, http://glfc.umiacs.umd.edu/index.shtml) and projected in UTM WGS84 Zone 19. Major structures of the investigated area in the Neuquén Basin [after *Cobbold et al.*, 1999; *Melnick et al.*, 2006; *Folguera et al.*, 2007; *Galland et al.*, 2007a]; MTB: Malargue Thrust Belt; BCFB: Barrancas Colorado Fold Belt; MTF: Main Thrust Front; AFTB: Agrio Fold and Thrust Belt; GFTB: Guanacos Fold and Thrust Belt; FMT: Filo Morado Thrust; CF: Carbonilla Fault; CL: Cortadera Lineament. Orientation and classification of the maximum horizontal stress are from *Guzman et al.* [2007]. The black dashed line on the west indicates the boundary between Chile and Argentina, the white line on the east delimits the east margin of the Neuquén basin. Inset: present-day plate tectonics setting of South America. The blue box locates the investigated area. The Nazca and Antarctic plates converge with South America at rates of 2 to 10 cm a^{-1} (numbered white arrows from *Cobbold et al.* [1999]). Steep segments of subducted Nazca slab correlate with Quaternary volcanoes of the North Volcanic Zone (NVZ), Central Volcanic Zone (CVZ), and South Volcanic Zone (SVZ). The image of South America is derived from GEOTOPO 30 (courtesy of the University of Maryland Global Land Cover Facility, http://glfc.umiacs.umd.edu/index.shtml).

N-S trending pop-up structures and thrusting coeval with the production of basaltic and silicic lavas associated with E-W trending eruptive fissures (dome and vent alignments). Alternatively, *Folguera et al.* [2008] interpreted the folds and inverse faulting affecting the products of Tromen volcano as minor structures accommodating the bulk crustal extensional strain between 3 and 1 Ma
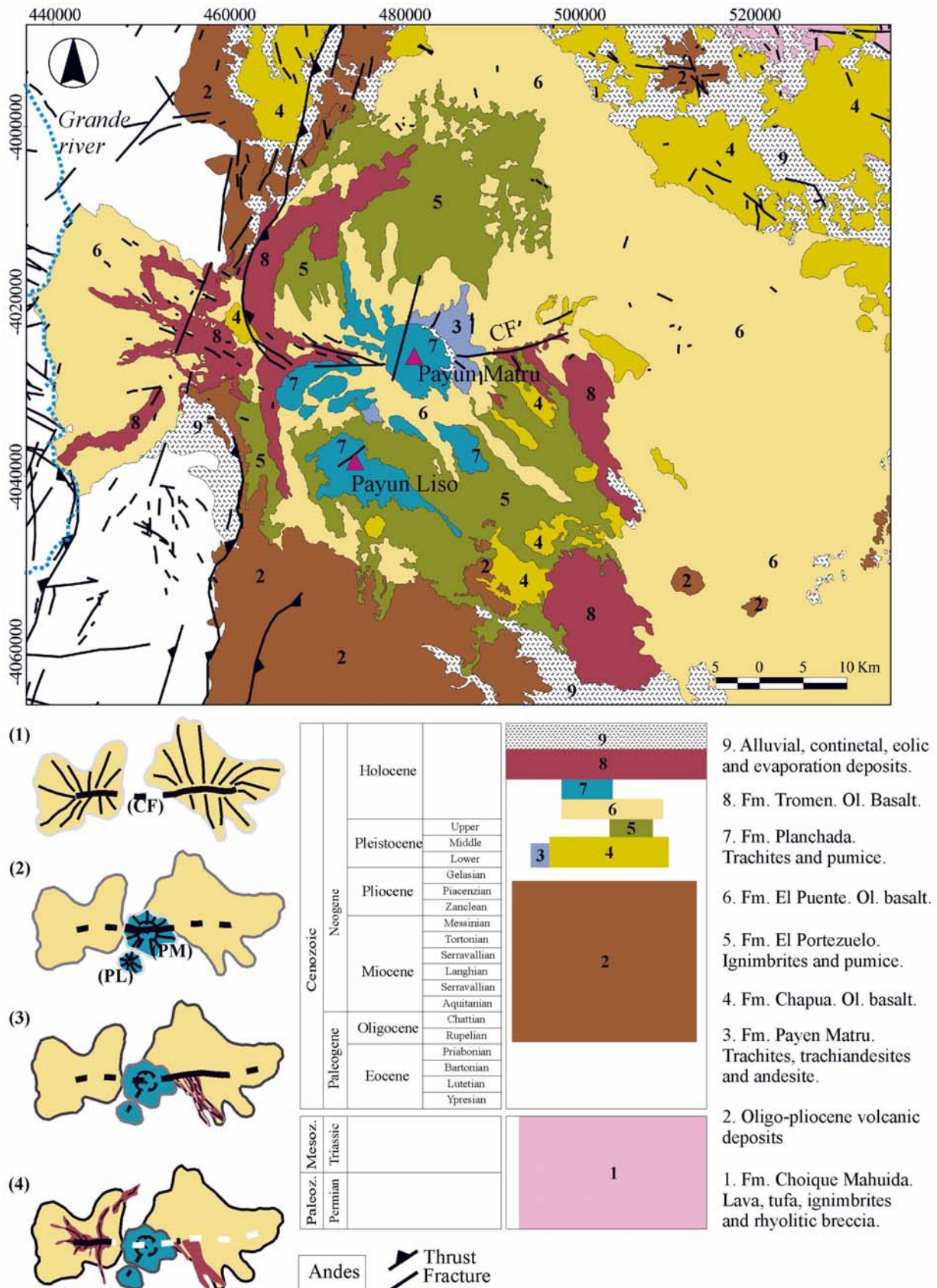
Figure 2

during a generalized E-W extension. Notably, both authors [*Galland et al.*, 2007a; *Folguera et al.*, 2008] report the occurrence of nearly E-W trending eruptive fissures encompassing the whole lifespan of the volcano; E-W eruptive fissure are the main structures also in the Payen Volcanic complex (see below). Considering that eruptive fissures tend to form normal to the minimum principal stress [e.g., *Nakamura*, 1977; *Tibaldi*, 1995], a regional E-W compression for the studied sector is coherent with the structures feeding the volcanism in that area. In this interpretation, the N-S trending grabens described in *Folguera et al.* [2008] may thus be interpreted as structures that accommodate extension on the hanging wall of regional N-S trending thrust systems. Moreover, the proposed scenario matches well the present stress field in the Nequén basin as observed by borehole breakouts data [*Guzman et al.*, 2007].

[6] At the latitude of the Payen Volcanic Complex, the crustal thickness can be derived from different geophysical data. The analysis of receiver functions data at 36°S of latitude, i.e., very close to the Payen Volcanic Complex, images a Moho depth of nearly 50 km [*Gilbert et al.*, 2006]. Broadband waveforms data from crustal earthquakes define a crust thickness in excess of 45 km at 36°S [*Alvarado et al.*, 2005; 2007]. In the latitude range 36°S–40°S, seismic data locate the Moho at a depth of 40 km in the Cordillera (71°W) with a Moho deepening (>45 km) further east [*Bhom et al.*, 2002]. The analysis of gravimetric anomalies along profiles at 39°S latitude (i.e., nearly 280 km south of the Payen Volcanic Complex) shows a Moho depth ranging from 45 to 50 km [*Folguera et al.*, 2007]. At the South American plate scale, from waveform joint inversion, a crust thickness greater than 40 km is calculated for the area at 36°30′S and 39°30′S [*Feng et al.*, 2007]. Moreover, forward modeling of the Bouger anomaly defines a crustal thickness >45 km for the studied area [*Tassara et al.*, 2006].

[7] Summarizing the above, at latitude 36°S–38°S in the retro-arc foreland of the central Andes, the currently active crust deformation is E-W contraction, as testified by coherent GPS, structural and borehole breakout data. Crustal shortening has been active since the late Pliocene and associated with active volcanism as testified by Tromen volcano. The Pleistocene to Recent Payen Volcanic Complex developed in this sector of the central Andes foreland, characterized by a crust thickness in the range of 45–50 km.

3. Payen Volcanic Complex

[8] The Payen Volcanic Complex is located at 35°S–37°S latitude and 68°W–70°W longitude. It is a Quaternary fissural volcanic structure, developed along an E-W, 70-km-long fault system known as Carbonilla Fault, inside the Andean back-arc Neuquén Basin [*Groeber*, 1938; *Ramos and Kay*, 2006; *Kay et al.*, 2006; *Germa et al.*, 2007]. Its stratigraphic basement is represented by the northernmost plateau of the Tertiary Patagonian basalts, defined as Palauco Formation by *González Díaz* [1972a].

[9] The activity of the Payen Volcanic Complex probably started during the Pleistocene, when basaltic lava shields with related scoria and spatter cones developed along two segments of the Carbonilla Fault system (Figure 2). These products partly correspond to the Morado Alto Formation by *González Díaz* [1972b] and partly to the Basalts III and IV of *Groeber* [1946]. The effusive activity of the eastern shield produced a large volume of olivine-basaltic lava flows [*Groeber*, 1929; 1946; *González Díaz*, 1972a, 1972b; *Núñez*, 1976]. Recently, these flows have been described as large fields of compound and single pahoehoe inflated, very long lava flows. The longest among these flows reaches distances of more than 180 km from the vents [*Pasquarè et al.*, 2005, 2008]. After this basaltic effusive activity a new widespread volcanic activity developed along the central sector of the Carbonilla Fault system (Figure 2), leading to the formation of two great trachytic and trachyandesitic stratovolcanoes, Payun Liso (36°30′34″S– 69°17′08″W) and Payun Matru (36°24′51″S– 69°12′22″W), respectively. While Payun Liso was not involved in any further relevant event, the original cone of Payun Matru volcano was partially destroyed by an 8-km wide caldera collapse (~168 ka [*Germa et al.*, 2007]). After the collapse, highly viscous trachytic and trachyandesitic lavas were erupted from intracalderic and extracalderic

Figure 2. (top) Geological map of the volcanic fissure (Carbonilla Fault; CF) and associated volcanoes Payun Matru, Payun Liso. (bottom right) Key legend for the geological map. (bottom left) Cartoon showing the evolution of the Payen Volcanic Complex. The proposed evolution and the geological map derive from a compilation of current geological maps (Carta Geologica de la Republica Argentina, scale 1:250000 [*Geological Survey of Argentina*, 2003a, 2003b]) by data from *Pasquarè et al.* [2008] and by field survey.

vents forming thick and levee-bordered flows, well described by *Llambías* [1966].

[10] The Carbonilla fault provided once more a very efficient feeding system, when a new phase of basaltic volcanism developed on both extremities of the fault itself (Figure 2). This younger phase of olivine-basaltic lava production was very noticeable in the western shield of the Payen Volcanic Complex, where large a'a' basaltic lava flows were outpoured in very recent times. The radiometric dating of one of the basaltic lava fields yields a K-Ar age of 0.40 ± 0.1 Ma. [*Melchor and Casadío*, 1999]; moreover, three cosmogenic 3He exposure ages on primary lava flow surfaces (at ∼36.31°S; 69.66°W) near the Rio Grande, indicate a late Pleistocene age in the range 37 ± 3–44 ± 2 ka for this unit [*Marchetti et al.*, 2006]. Finally, the latest a'a' lava flows are very young, as they have been reported by the local oral tradition dating back to colonial times [*González Díaz*, 1972b].

[11] Also along the eastern sector of the Carbonilla fault system both a'a' and pahoehoe, very young, olivine-basaltic lava flows were outpoured on the southeastern flank of the Payen Volcanic Complex, partly covering the older, very large lava fields. The very recent age of the volcanic activity along the eastern sector of the Payen Volcanic Complex is proved by the Holocene age of some cinder cones called "El Rengo Group" by *Inbar and Risso* [2001].

[12] The products of the Payen Volcanic Complex have a clear within-plate geochemical signature [*Kay et al.*, 2006, and references therein]. In particular, monogenetic cones show variation in silica content from 42.3 to 51.7 wt.%, and therefore can be mainly classified as basic. Some vents also erupted ultrabasic lavas [*Bertotto et al.*, 2006, and references therein].

[13] The volcanic products of the Payen Volcanic Complex are poorly deformed; few steeply dipping E-W trending extensional fractures have been measured on basaltic lava flows (Figure 3a). Permo-Triassic volcanic, volcaniclastic, and intrusive rocks (formations Aguas de los Burros, Choique Mahuida, and El Portillo group [*Geological Survey of Argentina*, 2003a]) crop out east and northeast of the volcanic field where they form the basement for the products of the Payen Volcanic Complex. Brittle deformation in these formations is characterized by NW-SE and N-S trending fractures and by pure extensional E-W fractures (Figure 3b). Cone alignments trend E-W (Figure 3c) as well

as the eruptive fissures (Figures 1 and 2). Field data thus indicate that E-W extensional fractures affect the young volcanic deposits of the Payen Volcanic Complex.

4. Spatial Distribution of Fractures and Vents

[14] The way in which fractures fill space (i.e., the spatial distribution of fractures) depends strictly on the spacing of fractures, which is correlated with the thickness of the fractured medium calculated on the basis of the stress saturation model [*Wu and Pollard*, 1995; *Gross et al.*, 1995; *Ackermann and Schlische*, 1997]. A robust way to define how fractures fill space is to analyze their self-similar clustering. The definition of self-similar clustering for the spatial correlation of fractures (i.e., computation of the fractal exponent, see *Bonnet et al.* [2001] and references therein) is performed for a range of lengths (the size range) between a lower and an upper cutoff. In its fundamental treatise, *Mandelbrot* [1982] suggested that there are upper and lower cutoffs for the scale-invariant characteristics of fractures (e.g., spacing, length, density) and that these are a function of mechanical layering and rock properties. This has been confirmed by laboratory experiments on normal fault populations, which suggest the presence of upper and lower cutoffs related to the thickness of the fractured layer [*Ackermann et al.*, 2001]. Moreover, the thickness of both sedimentary beds and the crust controls the scaling law of fractures and earthquakes [*Pacheco et al.*, 1992; *Davy*, 1993; *Ouillon et al.*, 1996].

[15] Volcanic eruption requires hydraulically open pathways that allow magmas to move upward from crustal or subcrustal reservoirs to the surface. The bulk permeability of the crust may be enhanced through fracturing; rock-fracturing processes allow the ascent of magma at rates that are akin to the timescale characterizing volcanic activity [*Rubin*, 1993; *Petford et al.*, 2000; *Canon-Tapia and Walker*, 2004]. A strong correlation between fractures and vent alignments has been identified in active Holocene volcanic fields (e.g., Iceland, Kamchatka); these geometric relationships have been ascribed to the exploitation of favorably oriented preexisting structures by the ascending magma [*Connor and Conway*, 2000, and references therein]. The feeder system of monogenetic apparatuses [see *Connor and Conway*, 2000] consists of dikes and each feeder may be used only one time, as the cooled magma seals the hydraulic pathway. This condition
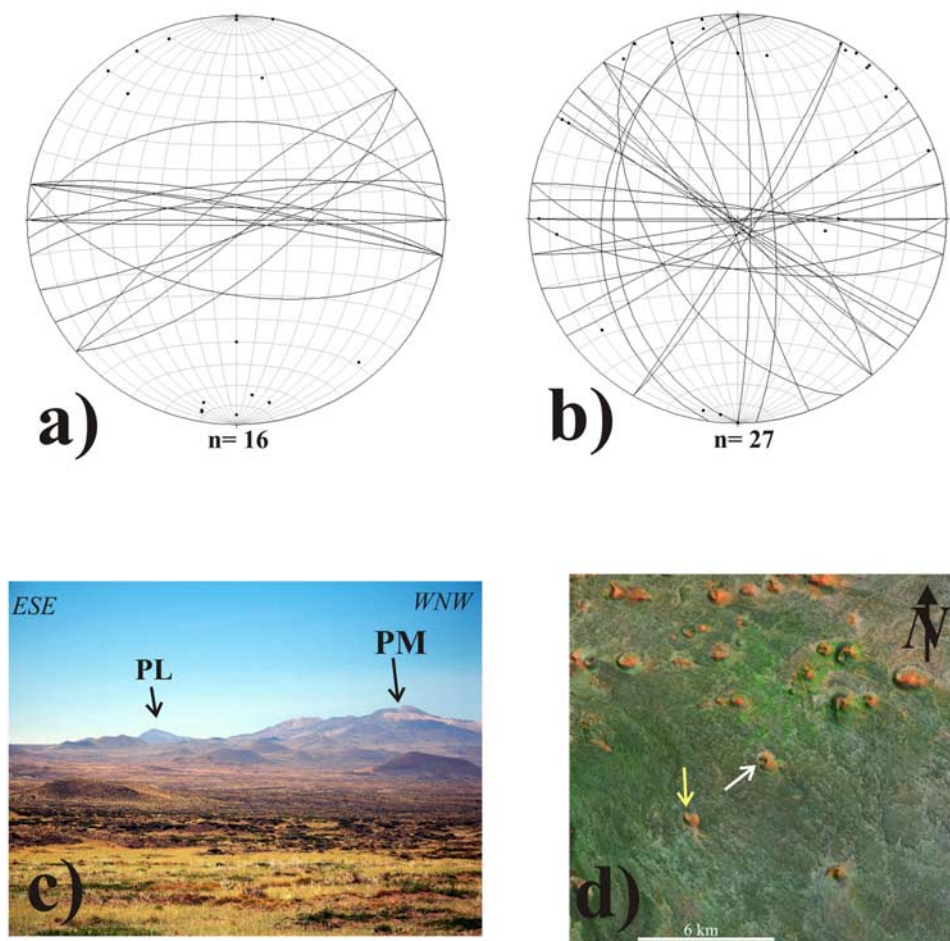
Figure 3. (a) Stereonet (lower hemisphere) of poles to fractures in the young lava flow of the Payen Volcanic Complex); n is the number of measurements. (b) Stereonet (lower hemisphere) of poles to fractures in the basement rocks of the Payen Volcanic Complex); n is the number of measurements. (c) Panoramic view of the northeastern slopes of the Payun Matru (PM), note the E-W alignment of cones. PL is Payun Liso volcano. The long side of the picture is about 22 km wide. (d) RGB False Color Composite of Landsat ETM image mosaic (courtesy of the University of Maryland Global Land Cover Facility, http://glfc.umiacs.umd.edu/index.shtml), band ETM + band 7 in the red channel, ETM + band 4 in the green channel, and ETM + band 2 in the blue channel. Projection: UTM 19, Datum: WGS84, pixels size = 14.25 m. In the image the breaching of cones has E-W (white arrow) and N-S (yellow arrow) directions.

is met in monogenetic vents (i.e., cinder and spatter cones) within volcanic fields. In the work of *Mazzarini* [2004] a simple model is developed for visualizing the relationship between vents and the geometric properties of fractures. This model assumes that the aperture of a fracture is greatest at its barycenter and that volcanic vents erupt at the point of maximum fracture aperture; the resulting vent distribution is thus closely linked to the hydraulic properties of both the crust and fractures.

[16] The connectivity of fractures is a critical feature controlling the fluid movement in the crust, as it defines the portion of the existing fracture network that hydraulically connects the system boundaries, allowing fluids to flow [e.g., *Renshaw*, 1999]. In a

rock volume the connected network is a subset of the existing fracture network [e.g., *Roberts et al.*, 1999], defined as the backbone in percolation theory [*Stauffer and Aharony*, 1992]. Hydraulic features of fractures such as fracture connectivity and aperture are scale invariant [*Bonnet et al.*, 2001]. In particular, the spatial clustering of a fracture network, represented as the fracture barycenter, has been directly linked to the hydraulic properties of the fracture network [*Bour and Davy*, 1999].

[17] Assuming a direct genetic and spatial link between fracture and vent [*Connor and Conway*, 2000; *Mazzarini*, 2004], scale invariance in vent distribution thus reflects the fractal properties of the connected part of a fracture network (i.e., the

backbone). The connected fracture network allows basaltic magma to rise to the surface from deep crustal or subcrustal reservoirs, passing through most or the whole of the crust. Analysis of the fractal character of the spatial distribution of vents can thus reveal the mechanical layering of the crust.

[18] Summarizing, the correlation between vent distribution and fracture network properties is such that the spatial distribution of vents may be studied in terms of self-similar (fractal) clustering [*Mazzarini*, 2004; *Mazzarini et al.*, 2004; *Mazzarini*, 2007], as in the case of fracture networks [*Bour and Davy*, 1999; *Bonnet et al.*, 2001]. Findings based on this approach suggest that for basaltic volcanic fields, (1) the distribution of monogenetic vents is linked to the mechanical layering of the crust, (2) vents tend to cluster according to a power law distribution, and (3) the range of lengths over which the power law distribution is defined, is characterized by an upper cutoff that approximates the thickness of the fractured medium (crust). This correlation has been studied in volcanic fields within extensional continental settings in back arcs, such as in southernmost Patagonia [*Mazzarini and D'Orazio*, 2003] and in continental rifts such as the Ethiopian Rift System [*Mazzarini*, 2004] and in the Afar Depression [*Mazzarini*, 2007].

[19] It is noteworthy that the characteristic power law exponents, describing the spatial distribution (clustering) of a given fracture network, increase as the fracture network evolves [*Barton*, 1995]. Moreover, newly formed fault systems in a continental rift are more clustered than older ones [*Giaquinta et al.*, 1999], suggesting that new fractures in prefractured crust have higher exponent values than older ones. *Mazzarini and D'Orazio* [2003] tested this model in southernmost Patagonia (~52°S of latitude), in a continental back-arc setting using Quaternary to recent volcanic products to confirm the relative chronology of the detected structural trends. Moreover, it has been demonstrated that the frequency/length distribution evolves from power law to exponential and eventually reaches a saturation level for very high strains [*Gupta and Scholz*, 2000; *Spyropoulos et al.*, 2002, *Scholz*, 2002]. Hence, these parameters can be used to assess the relative stage of evolution and maturity of a fracture network.

4.1. Data Acquisition

[20] Landsat 7 ETM + data were used to identify and map volcanic vents and fractures [*Goward et al.*, 2001] (http://landsathandbook.gsfc.nasa.gov/

handbook.html). A mosaic of 29 ETM false-color composite images was used to map large portion of the Andes Foothills (courtesy of the University of Maryland Global Land Cover Facility, http://glfc.umiacs.umd.edu/index.shtml). The images are georeferenced to the UTM projection (zone 19 S - datum WGS84) and displayed as RGB false color composites (with ETM + band 7 in the red channel, ETM+ band 4 in the green channel, and ETM + band 2 in the blue channel). The original spatial resolution of Landsat ETM + images is 30 × 30 m. The 15 × 15 m spatial resolution of the Landsat ETM + mosaic was obtained through a color transform using the 15 × 15 m geometric resolution of the Landsat ETM + panchromatic band [*Janza et al.*, 1975; *Vrabel*, 1996].

[21] The image mosaic clearly shows volcanic features as well as fractures and faults (Figure 4) and enables to map fractures and vents in a GIS environment (ArcView 3.3).

[22] Structural analysis of satellite images is based on the detection of rectilinear features (lineaments) of regional to continental scale. Lineaments consist in sharp tonal differences and alignments of morphological features (e.g., volcanic cones, triangular facets, portions of streams, aligned ridges and crests). Within tectonically active areas, lineaments usually match the fracture network and the main fracture patterns [e.g., *Abebe et al.*, 1998]. We assume that lineaments are the intersection of the fracture network with the Earth's surface; we thus consider lineaments as traces of fractures and will hereafter refer to lineaments as fractures. In the Payen Volcanic Complex, 1098 fracture traces were detected and stored in the GIS, as well as the UTM coordinates of their extreme points, which allows for lineament azimuth to be calculated. The definition of main fracture sets is obtained by analyzing the azimuth frequency distribution [*Wise et al.*, 1985; *Abebe et al.*, 1998; *Zakir et al.*, 1999]. Since the Landsat image used for this study is illuminated from the NE, a slight overestimation of the NW-SE lineaments is expected.

[23] Both vents and fractures were then analyzed in terms of their self-similar clustering and spacing. The location of vents was identified on the satellite images with an accuracy of one pixel (i.e., 15 × 15 m). Moreover, the relationships between vents and fractures are well imaged by the synoptic view of satellite images. Up to 879 vents (coded as "all-vents" data set) with diameter larger than 200 m were identified, and their coordinates were stored in the GIS. This
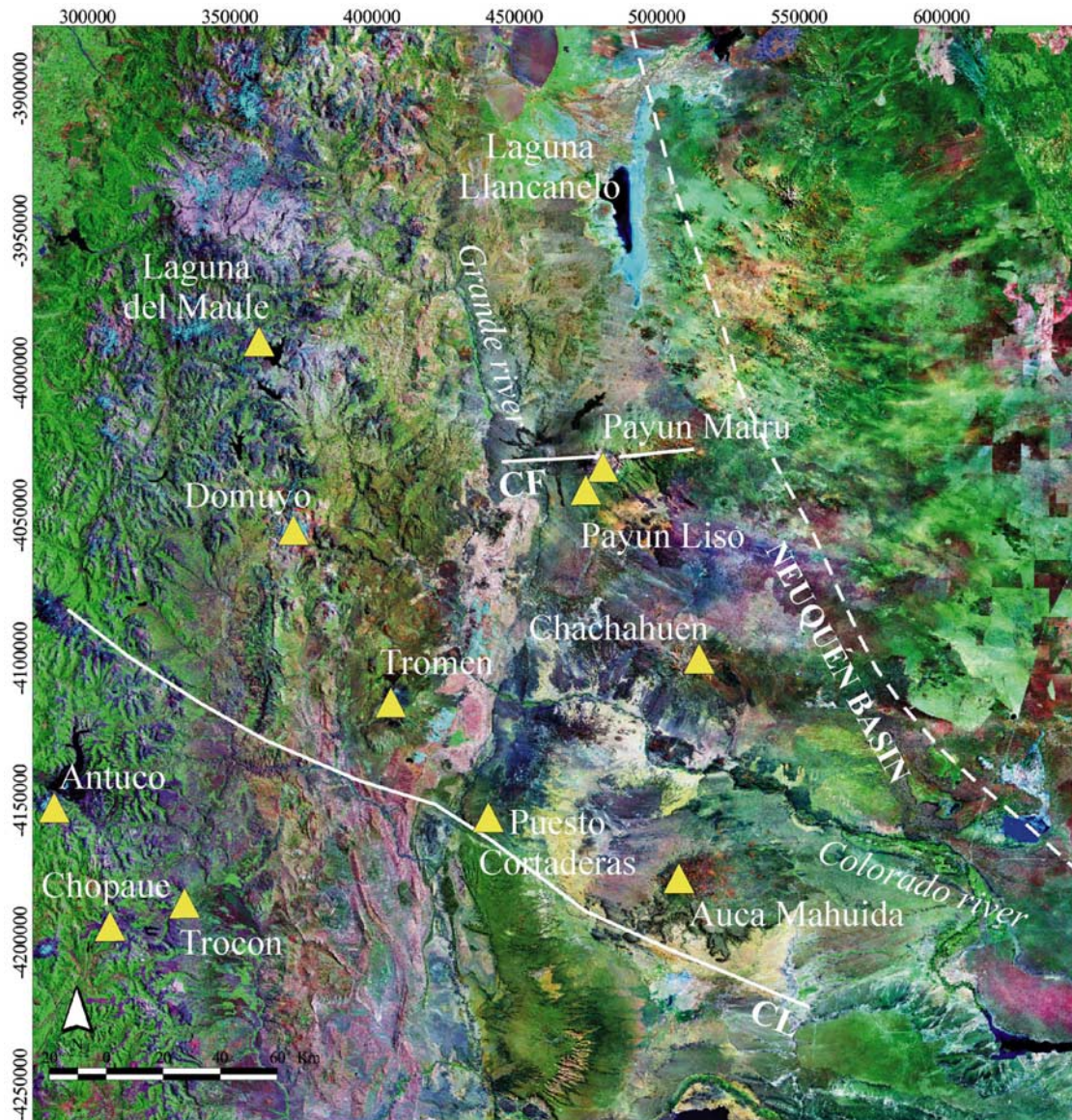
Figure 4. RGB False Color Composite of Landsat ETM image mosaic (courtesy of the University of Maryland Global Land Cover Facility, http://glfc.umiacs.umd.edu/index.shtml), band ETM + band 7 in the red channel, ETM + band 4 in the green channel, and ETM + band 2 in the blue channel. Projection: UTM 19, Datum: WGS84, pixels size = 14.25 m. In the image fault trace, vents and caldera structure are apparent. CF: Carbonilla Fault; CL: Cortadera Lineament.

allowed mapping of the density of vents (number of vents per unit area).

[24] Cinder and spatter cones represent the most common volcanic features in the Payen Volcanic Complex (Figures 1 and 2) and are often affected by breaching. The breaching of cinder cones derives from the eruption of an associated lava flow and is defined as the removal of material from the cone due to erosional, gravitational, or volcanic mechanisms, such that the interior of the cone is exposed. Clear example of E-W and N-S directed

breaching are observed in the Payen Volcanic Complex (Figure 3d). The azimuths of the breaching of 114 vents were recorded and analyzed, as they are structurally related to the feeders' trends [e.g., *Tibaldi*, 1995]. Since the southernmost part of the volcanic field is characterized by the occurrence of late Miocene andesitic to rhyolitic domes (i.e., the Chachauén Field [*Kay et al.*, 2006]), and in order to avoid the possibility to select non-basaltic vents, a subset of 675 vents (coded as "Payun-Matru" data set), located only in the

Table 1. Statistics of the Spacing and Self-Similar Clustering for Fractures and Vents[a]

Data Set	n	sp (km)	sp σ (km)	CV	Lco (km)	Uco (km)	D	R^2
Fractures	1098	2.54	2.82	1.11	1.5 ± 0.5	48.1 ± 4.5	1.623 ± 0.005	0.999
All vents	879	1.27	1.89	1.48	0.9 ± 0.2	49.3 ± 3.3	1.325 ± 0.004	0.999
Payun-Matru	675	1.19	1.95	1.64	0.8 ± 0.4	47.1 ± 3.6	1.332 ± 0.007	0.999

[a] Here n is number of points; sp is average spacing; sp. σ is standard deviation of spacing; CV is coefficient of variation; Lco is lower cutoff; Uco is upper cutoff; D is correlation exponent; and R^2 is coefficient of correlation.

central and northern part of the volcanic field (around the Payun Matru and the Laguna Llancanelo) was created. The Payun-Matru data set thus is completely comprised in the volcanic fields described by *Inbar and Risso* [2001].

4.2. Methods

[25] Vents and fractures in the Payen Volcanic Complex were analyzed in terms of self-similar clustering and mean separation [*Mazzarini*, 2004, 2007]; vents density was also investigated.

[26] The spatial clustering of vents/fractures was analyzed by calculating the correlation exponent *D* [*Bonnet et al.*, 2001]. A two-point correlation function method was used to measure the fractal dimension of the vent/fracture population. For a population of N points (vent centers or fracture barycenters), the correlation integral *C(l)* is defined as the correlation sum that accounts for all the points at a distance of less than a given length *l* [*Bonnet et al.*, 2001, and references therein]. In this approach, the term *C(l)* is computed as:

$$C(l) = 2N(l)/N(N-1) \qquad (1)$$

where *N(l)* is the number of pairs of points whose distance is less than *l*. If scaling holds, equation (1) is valid, and the distribution defines a power law of the form:

$$C(l) = Al^{-D} \qquad (2)$$

the slope of the curve in a *log(C(l))* versus *log(l)* diagram yields the *D* exponent.

[27] The distance interval over which equation (2) is valid is defined by the size range. For each analysis, the size range of samples is in turn defined by a plateau in the local slope versus *log(l)* diagram: the wider the range the better the computation of the power law distribution [*Walsh and Watterson*, 1993]. The size range over which equation (2) is valid is bounded between two values defined as the lower and the upper cutoffs

[e.g., *Ackermann et al.*, 2001; *Mazzarini*, 2004]. The derivation of the cutoffs is a crucial point and is generally not trivial, especially when the local slope does not show a regular and wide plateau. The choice of the zones where the plateau is well defined and the determination of the lower and upper cutoffs are done according to *Mazzarini* [2004] by selecting the wider length range for which the correlation between *log(l)* and local slope is greatest. Truncation and censoring affect the computation of the fractal distribution for fractures [*Bonnet et al.*, 2001] and cones [*Mazzarini*, 2004]. In order to fit the data for a scale-range probably not affected by these effects, at least 150–200 objects (fracture barycenters and cones in this case) must be analyzed [*Bonnet et al.*, 2001; *Bour et al.*, 2002].

[28] The distribution of fractures and vents in the Payen Volcanic Complex was also analyzed in terms of fractures/vents separation. Separation (or spacing) is analyzed by computing the average minimum distance between fractures/vents. The coefficient of variation CV [*Gillespie et al.*, 1999, and references therein], defined as:

$$CV = s/m \qquad (3)$$

where *s* is the standard deviation and *m* is the mean, describes the degree of clustering. *CV > 1* indicates clustering of fractures/vents, *CV = 1* indicates a random or Poisson distribution, and *CV < 1* indicates anticlustering (a homogeneous distribution).

[29] In order to analyze the density of vents taking into account their spatial distribution, the Vent Closeness method was introduced [*Mazzarini*, 2007]. This method computes the number of vents within a radius *r* centered on each vent of the data set; a search radius of 2.5 km has been used being twice the mean vent spacing (Table 1). The resulting vent density for each data set is the average of the measures relative to all the vents in the data set.
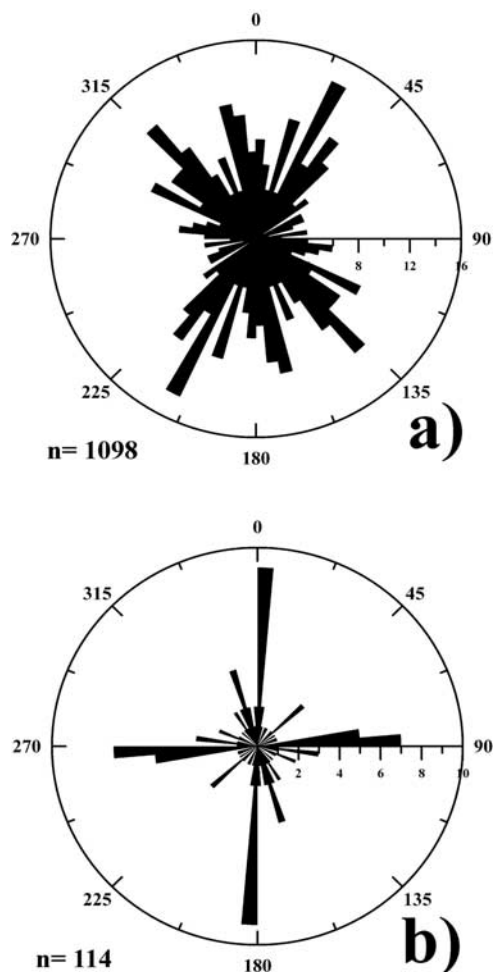
Figure 5. Rose diagrams of azimuth frequency distribution: (a) fractures (1098) and (b) cone breaching (114).

4.3. Results

[30] The azimuth distribution of the detected fractures is characterized by five main peaks; NE-SW, NW-SE, and NNW-SSE are the principal trends; minor N-S and E-W trends are also present (Figure 5a). As a whole, the detected principal trends match the structural grain of the Neuquén Basin as well as the main features in the basement fabrics as derived by aeromagnetic data [*Cobbold et al.*, 1999; *Cobbold and Rossello*, 2003; *Mosquera and Ramos*, 2006, and references therein]. The NW-SE trend may be associated with structures related to the Triassic rifting in Southern Patagonia, whereas the NE-SW and the N-S trends may be associated with structures developed during the Eocene deformation resulting in right-lateral transpression and strike-slip faulting [*Cobbold and Rossello*, 2003] and in the formation of NE trending

bitumen dikes [*Cobbold et al.*, 1999]. The observed E-W trend in the fracture network is consistent with the stress field in the area [e.g., *Guzman et al.*, 2007]. E-W tensional fractures are also observed in the very young lava flows of the Payen Volcanic Complex (Figure 3); also the eruptive fissures in the studied area as well as at the Tromen volcano show this trend [*Galland et al.*, 2007a; *Folguera et al.*, 2008]. Therefore E-W fractures have been considered to be mainly extensional structures. Fracture spacing has an average value of 2.54 km with a coefficient of variation CV of 1.11, suggesting a clustered distribution of fractures (Table 1).

[31] The whole population of vents of the Payen Volcanic Complex (all-vents data set) is confined within a strip 150 km wide and 300 km long starting just a few kilometers north of the Cortaderas lineament and ending just north of the Laguna Llancanello (Figure 6). Spacing of vents in this data set has an average value of 1.27 km, with a $CV = 1.48$, suggesting a well clustered distribution (Table 1). Vent density has an average of 0.2 vent/km^2, with a maximum of 0.7 vent/km^2. The maximum vent density is localized along the Carbonilla fault and close to the Payun Matru volcano (Figure 7). Vents of the Payun-Matru data set show an average spacing of 1.19 km, somewhat lower than the spacing of the "all-vents" data set (Table 1). Also this data set shows a well defined clustering, as suggested by $CV = 1.64$. This data set comprises the zones with high vent density (Figures 6 and 7).

[32] The breaching of vents (Figures 3d and 5b) shows an azimuth distribution with two well defined main peaks, one trending nearly E-W and the other N-S. Most of the breached cones are on slopes less than 4°, thus minimizing the effect of bedrock slope and maximizing the control on cone breaching by feeding fractures [e.g., *Tibaldi*, 1995]; the breaching trends are coherent with an E-W main trend for the vent feeders, thus paralleling the Carbonilla Fault.

[33] In terms of the self-similar clustering both fractures and vents in the Payen Volcanic Complex have a well defined fractal (power law) distribution defined over one order of magnitude (Table 1 and Figure 8).

[34] The fracture data set shows a correlation exponent $D = 1.623 \pm 0.005$, in the range defined by a lower cutoff (Lco) of 1.5 ± 0.5 km and an upper cutoff (Uco) of 48.1 ± 4.5 km. The "all-vents" data set has an exponent $D = 1.325 \pm 0.004$,
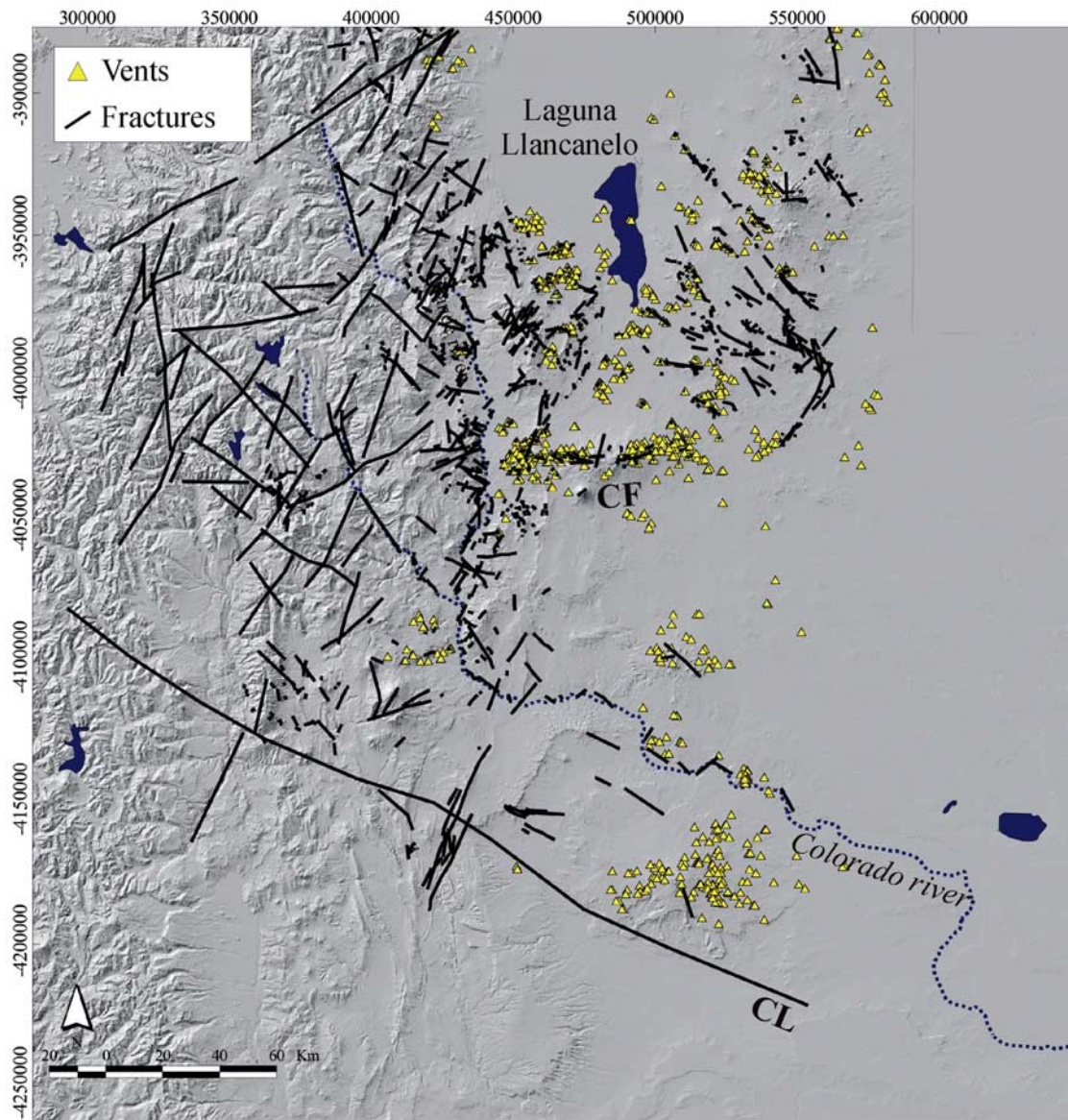
Figure 6. Map of lineaments and cones in the Payen Volcanic Complex. CF: Carbonilla Fault; CL: Cortadera Lineament.

defined in the range $0.7 \pm 0.2 - 49.3 \pm 3.3$ km. The Payun-Matru data set shows an exponent $D = 1.333 \pm 0.007$ with $Lco = 0.8 \pm 0.4$ km and $Uco = 47.1 \pm 3.6$ km.

5. Discussion

[35] In the Andean foreland between 35°S and 37°30′S, back-arc basaltic volcanism has been active from the Late Pliocene to the Holocene, as testified by the occurrence of the Payen Volcanic Complex and Tromen Volcano [*Galland et al.*, 2007a; *Folguera et al.*, 2008]. In the Payen Volcanic Complex, basaltic lavas are the most volu-

minous products, associated in some places with andesitic to rhyolitic products. This sequence is quite similar to what is observed at Tromen Volcano [*Galland et al.*, 2007a]. In the Payen Volcanic Complex, structural features (eruptive fissures and cone breaching) mainly trend E-W, in complete agreement with the stress field, produced by a regional scale E-W shortening [*Guzman et al.*, 2007]. This suggests that these features might have controlled the vent distribution in the Payen Volcanic Complex from the Early Pleistocene to the Present.

[36] The self-similar clustering of fractures has an exponent $D \sim 1.62$, very close to the correlation
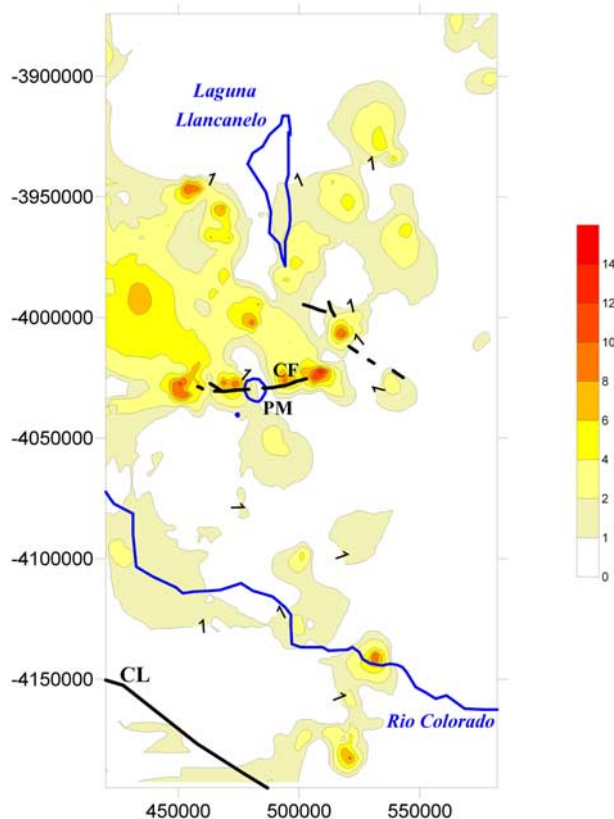
Figure 7. Map of the vent density in the Payen Volcanic Complex. The grid spacing is 2.5 km. CF: Carbonilla Fault; CL: Cortadera Lineament; PM: Payun Matru.

exponent of the S. Andreas Fault System ($D \sim 1.65$ [*Bour and Davy*, 1999]), and comprised between the value displayed by the fracture network in the Main Ethiopian rift ($D \sim 1.45–1.56$ [*Giaquinta et al.*, 1999]) and the value ($D \sim 1.80$) computed for the jointed Devonian sandstones in the Hornelen basin, in western Norway [*Bour et al.*, 2002].

[37] Field and laboratory experimental data suggest that the fractal distribution of the fracture network is controlled by the mechanical layering of the crust, showing cutoff values of power law clustering related to the thickness of sedimentary basins or the whole crust thickness [*Pacheco et al.*, 1992; *Davy*, 1993; *Ouillon et al.*, 1996; *Ackermann et al.*, 2001]. In southern Patagonia, the back-arc basaltic Paly Aike volcanic field shows a well developed fracture network with a correlation exponent $D \sim 1.74$ defined over a size range with an upper cutoff well fitting the crust thickness [*Mazzarini and D'Orazio*, 2003].

[38] In the Payen Volcanic Complex the upper cutoffs for all the data sets (fractures and vents)

converge toward a value of about 48–49 km, which in turn approximately corresponds to the crustal thickness in the area (45–50 km, suggested by independent geophysical data). In this sector of the Andes, such a crustal thickness of about 45–50 km, derived from analysis of the vent self-similar clustering and from independent geophysical data, is more coherent with general crustal shortening then crustal extension. Variations in the subducting-slab geometries lead to changes in time and space of the crustal stress state (compression versus extension) in the 35°S–39°S latitude range as proposed by *Folguera et al.* [2006]. The proposed compressional setting for the Payen Volcanic Complex as well as for Tromen volcano [*Galland et al.*, 2007a] could be hence associated to a much more complex geometry of the subducted slab and to a southward shift of the zone of crustal attenuation due to the changes in the geometry of the Benioff zone [*Folguera et al.*, 2006].

[39] Despite the within-plate geochemical signature of the erupted basalts at the Payen Volcanic Complex [*Kay et al.*, 2006; *Bertotto et al.*, 2006; *Pasquarè et al.*, 2008], the observed structural setting suggests that this volcanism was and is still active during crustal shortening, in contrast with the crustal extension setting proposed by *Kay et al.* [2006, and references therein]. Noteworthy, in such a compressive deformation regime, voluminous alkaline basaltic lava flows were erupted, associated with a large number of monogenetic cones [e.g., *Pasquarè et al.*, 2008]. A question rises now: Do we need crustal extension to produce within-plate lavas? Or do within-plate lavas generate from a very heterogeneous mantle and are successively drained by crustal scale fractures? The answer to these questions is far beyond the aim of this contribution; nevertheless we note that also the origin of hot spot lava has been recently questioned [*Meibom*, 2008; *Luguet et al.*, 2008].

6. Conclusions

[40] In the Andean foreland between 35°S and 37°30′S back-arc basaltic volcanism (the Payen Volcanic Complex) is testified by the occurrence of shield volcanoes, E-W eruptive fissures, monogenetic cones, and large basaltic lava flows. Similarly to Tromen Volcano [*Galland et al.*, 2007a; *Folguera et al.*, 2008], also at the Payen Volcanic Complex basaltic lavas are the most voluminous products and are associated with andesitic to rhyolitic products. The eruptive fissures, cone breaching and recent brittle deformation (fractures) trend
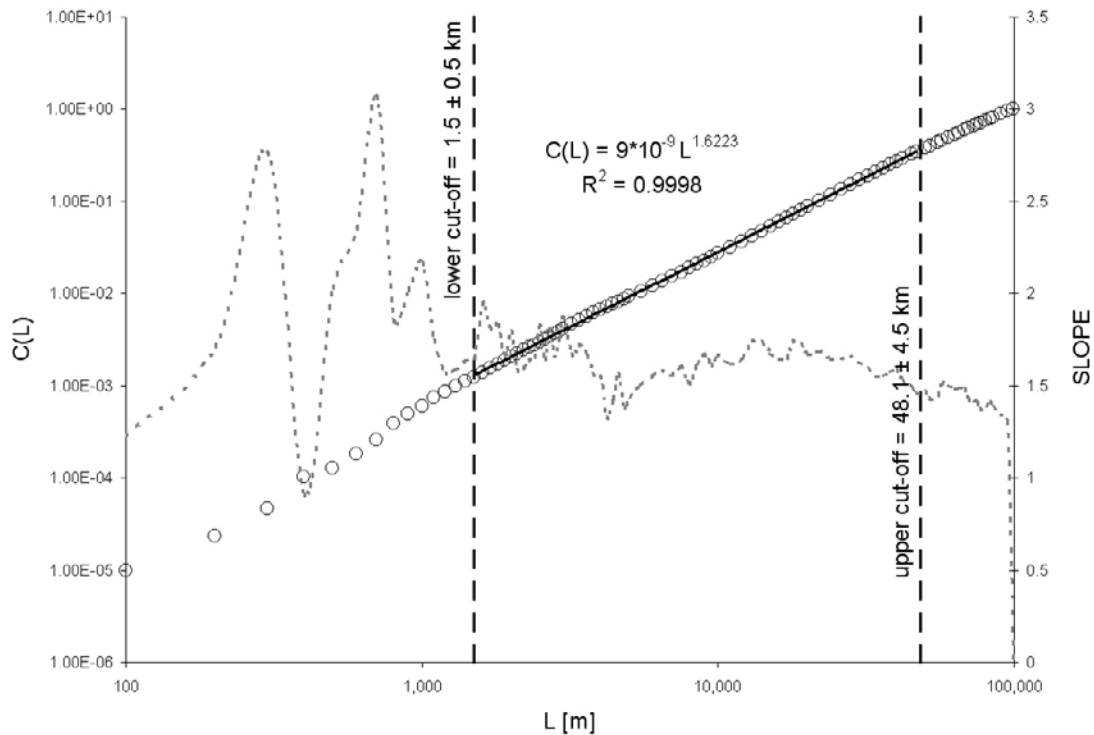
Figure 8. Plot of log(L) versus log(C(L)) for the Payun-Matru data set (open circle) and for the respective local slopes. Vertical black lines mark the upper and lower cutoffs of the size ranges of data set, for the local slope plot. The slope of the curves is the correlation exponent (D).

E-W, well matching the actual regional scale E-W shortening derived by borehole breakouts analysis [*Guzman et al.*, 2007].

[41] The monogenetic vents (about 890) as well as the fracture network in the Payen Volcanic Complex show self-similar clustering over size ranges greater than one order of magnitude (Table 1).

[42] Noteworthy, in a context of crustal shortening, a good correlation exists between the upper cutoffs of fractures' and vents' power law distributions (~48 km) and the crustal thickness (45–50 km) derived from geophysical data. As previously observed in extensional tectonic settings along the East African Rift System [*Mazzarini*, 2004, 2007] and in southern Patagonia [*Mazzarini and D'Orazio*, 2003], also in the Payen Volcanic Complex area the thickness of the crust scales as the upper cut-off defining the power law distribution of monogenetic vents.

[43] In general, we propose that the self-similar clustering of basaltic vents (and in particular the upper cutoff value), which is intimately linked to the network of hydraulically connected fractures, could be used as a proxy for the crust thickness, irrespectively of the tectonic regime of the area.

Acknowledgments

References

Abebe, T., F. Mazzarini, F. Innocenti, and P. Manetti (1998), The Yerer-Tullu Wellel volcanotectonic lineament: A transtensional structure in central Ethiopia and the associated magmatic activity, *J. Afr. Earth Sci.*, *26*, 135–150, doi:10.1016/S0899-5362(97)00141-3.

Ackermann, R. V., and R. W. Schlische (1997), Anticlustering of small normal faults around larger faults, *Geology*, *25*, 1127–1130, doi:10.1130/0091-7613(1997)025<1127:AOSNFA>2.3.CO;2.

Ackermann, R. V., R. W. Schlinsche, and M. O. Withack (2001), The geometric and statistical evolution of normal fault systems: An experimental study of the effects of mechanical layer thickness on scaling laws, *J. Struct. Geol.*, *23*, 1803–1819, doi:10.1016/S0191-8141(01)00028-1.

Alvarado, P., S. Beck, G. Zandt, M. Araujo, and E. Triep (2005), Crustal deformation in the south-central Andes back-arc terranes as viewed from regional broad-band seismic waveform modelling, *Geophys. J. Int.*, *163*, 580–598, doi:10.1111/j.1365-246X.2005.02759.x.

Alvarado, P., S. Beck, and G. Zandt (2007), Crustal structure of the south-central Andes Cordillera and backarc region from regional waveform modelling, *Geophys. J. Int.*, *170*, 858–875, doi:10.1111/j.1365-246X.2007.03452.x.

Barton, C. C. (1995), Fractal analysis of scaling and spatial clustering of fractures, in *Fractals in the Earth Sciences*, edited by C. C. Barton and P. R. La Pointe, pp. 141–178, Plenum, New York.

Bertotto, G. W., E. A. Bjerg, and C. A. Cingolani (2006), Hawaiian and Strombolian style monogenetic volcanism in the extra Andean domain of central-west Argentina, *J. Volcanol. Geotherm. Res.*, *158*, 430–444, doi:10.1016/j.jvolgeores.2006.08.001.

Bohm, M., S. Luth, H. Echtler, G. Asch, K. Bataille, C. Brun, A. Rietbrock, and P. Wigger (2002), The southern Andes between 36° and 40°S latitude: Sesimicity and average seismic velocities, *Tectonophysics*, *356*, 275–289, doi:10.1016/S0040-1951(02)00399-2.

Bonnet, E., O. Bour, N. E. Odling, P. Davy, I. Main, P. Cowie, and B. Berkowitz (2001), Scaling of fracture systems in geological media, *Rev. Geophys.*, *39*, 347–383, doi:10.1029/1999RG000074.

Bour, O., and P. Davy (1999), Clustering and size distribution of fault patterns: Theory and measurements, *Geophys. Res. Lett.*, *26*, 2001–2004, doi:10.1029/1999GL900419.

Bour, O., P. Davy, C. Darcel, and N. Odling (2002), A statistical scaling model for fracture network geometry, with validation on a multiscale mapping of a joint network (Hornelen Basin, Norway), *J. Geophys. Res.*, *107*(B6), 2113, doi:10.1029/2001JB000176.

Brooks, B. A., M. Bevis, R. Smalley Jr., E. Kendrick, R. Manceda, E. Lauria, R. Maturama, and M. Araujo (2003), Crustal motion in the southern Andes (26°–36°S): Do the Andes behave like a microplate?, *Geochem. Geophys. Geosyst.*, *4*(10), 1085, doi:10.1029/2003GC000505.

Canon-Tapia, E., and G. P. L. Walker (2004), Global aspects of volcanism: The perspectives of "plate tectonics" and "volcanic systems,", *Earth Sci. Rev.*, *66*, 163–182, doi:10.1016/j.earscirev.2003.11.001.

Clavero, J. E., R. S. J. Sparks, M. S. Pringle, E. Polanco, and M. C. Gardeweg (2004), Evolution and volcanic hazards of Taapaca Volcanic Complex, Central Andes of Northern Chile, *J. Geol. Soc.*, *161*, 603–618, doi:10.1144/0016-764902-065.

Cobbold, P. R., and E. A. Rossello (2003), Aptian to recent compressional deformation, foothills of the Neuquén Basin, *Argentina, Mar. Pet. Geol.*, *20*, 429–443, doi:10.1016/S0264-8172(03)00077-1.

Cobbold, P. R., M. Diraison, and E. A. Rossello (1999), Bitumen veins and Eocene transpression, Neuquén Basin, Argentina, *Tectonophysics*, *314*, 423–442, doi:10.1016/S0040-1951(99)00222-X.

Connor, C. B., and F. M. Conway (2000), Basaltic volcanic fields, in *Encyclopedia of Volcanoes*, edited by H. Sigurdsson, pp. 331–343, Academic, New York.

Davy, P. (1993), On the frequency-length distribution of the San Andreas fault system, *J. Geophys. Res.*, *98*, 12,141–12,151, doi:10.1029/93JB00372.

Feng, M., S. van der Lee, and M. Assumpção (2007), Upper mantle structure of South America from joint inversion of waveforms and fundamental mode group velocities of Rayleigh waves, *J. Geophys. Res.*, *112*, B04312, doi:10.1029/2006JB004449.

Folguera, A., V. A. Ramos, R. L. Hermanns, and J. Naranjo (2004), Neotectonics in the foothills of the southernmost central Andes (37°–38°S): Evidence of strike-slip displace-ment along the Antiñir-Copahue fault zone, *Tectonics*, *23*, TC5008, doi:10.1029/2003TC001533.

Folguera, A., T. Zapata, and V. A. Ramos (2006), Late Cenozoic extension and the evolution of the Neuquén Andes, in Evolution of an Andean Margin: A Tectonic and Magmatic View from the Andes to the Neuquen Basin (35°–39°S lat), edited by S. M. Kay and V. A. Ramos, *Geol. Soc. Am. Spec. Pap.*, *407*, 267–285.

Folguera, A., A. Introcaso, M. Giménez, F. Ruiz, P. Martinez, C. Tunstall, E. G. Morabito, and V. A. Ramos (2007), Crustal attenuation in the Southern Andean retroarc (38°–39°30′S) determined from tectonic and gravimetric studies: The Lonco-Luan asthenospheric anomaly, *Tectonophysics*, *439*, 129–147, doi:10.1016/j.tecto.2007.04.001.

Folguera, A., G. Bottesi, T. Zapata, and V. A. Ramos (2008), Crustal collapse in the Andean backarc since 2 Ma: Tromen volcanic plateau, southern Central Andes (36°40′–37°30′S), *Tectonophysics*, doi:10.1016/j.tecto.2007.12.013, in press.

Galland, O., E. Hallot, P. R. Cobbold, and G. Ruffet (2007a), Volcanism in compressional Andean setting: A structural and geochronological study of Tromen volcano (Neuquén province, Argentina), *Tectonics*, *26*, TC4010, doi:10.1029/2006TC002011.

Galland, O., P. R. Cobbold, and E. Hallot (2007b), Rise and emplacement of magma during horizontal shortening of the brittle crust: Insights from experimental modelling, *J. Geophys. Res.*, *112*, B06402, doi:10.1029/2006JB004604.

Geological Survey of Argentina (2003a), Carta geologica de la republica Argentina, hoja agua escondida, scale 1:250.000, Buenos Aires.

Geological Survey of Argentina (2003b), Carta geologica de la republica Argentina, hoja barrancas, scale 1:250.000, Buenos Aires.

Germa, A., X. Quidelleur, P. Y. Gillot, and P. Tchilinguirian (2007), Volcanic evolution of the back-arc complex of Payun Matru (Argentina) and its geodynamic implications for caldera-forming eruption in a complex slab geometry setting, paper presented at International Union of Geodesy and Geophysics 2007, Perugia, Italy.

Giaquinta, A., S. Boccaletti, M. Boccaletti, L. Piccardi, and F. T. Arecchi (1999), Investigating the fractal properties of geological fault system: The Main Ethiopian Rift case, *Geophys. Res. Lett.*, *26*, 1633–1636, doi:10.1029/1999GL900319.

Gilbert, H., S. Beck, and G. Zandt (2006), Lithospheric and upper mantle structure of central Chile and Argentina, *Geophys. J. Int.*, *165*, 383–398, doi:10.1111/j.1365-246X.2006.02867.x.

Gillespie, P. A., J. D. Johnston, M. A. Loriga, K. J. W. McCaffrey, J. J. Walsh, and J. Watterson (1999), Influence of layering on vein systematics in line samples, in *Fractures, Fluid Flow and Mineralization*, edited by K. J. W. McCaffrey, L. Lonergan, and J. J. Wilkinson, *Geol. Soc. London Spec. Publ.*, *155*, 35–56.

González Díaz, E. F. (1972a), Descripción Geológica de la Hoja 30 e (Agua Escondida), Provincias de Mendoza y La Pampa, *Bol. 135*, Serv. Nac. Minería y Geol., Buenos Aires.

González Díaz, E. F. (1972b), Descripción Geológica de la Hoja 30 d (Payún-Matru), Provincia de Mendoza, *Bol. 130*, Dir. Nac. de Geol. y Minería, Buenos Aires.

Goward, S. N., J. G. Masek, L. Darrel, D. L. Williams, J. R. Irons, and R. J. Thompson (2001), The Landsat 7 mission Terrestrial research and applications for the 21st century, *Remote Sens. Environ.*, *78*, 3–12, doi:10.1016/S0034-4257(01)00262-0.

Groeber, P. (1929), Líneas fundamentales de la Geología del Neuquén, sur de Mendoza y regiones adyacentes, *Publ. 58*, Direcc. Gral. Minas, Geol. Hidrol., Buenos Aires.

Groeber, P. (1938), Mapa geologico de la Gobernacion del Neuquén, fundamentales de la Geología del Neuquén, Territorio Nacional del Neuquén, *Map 12*, pp. 17–31, scale 1:1000000, Com. Nac. de Climatol. y Agric., Buenos Aires.

Groeber, P. (1946), Observaciones geológicas a lo largo del meridiano 70.1 Hoja Chos Malal, *Soc. Geol. Argentina, Ser. C, 1*, 1–174.

Gross, M. R., M. P. Fischer, T. Engelder, and R. J. Greenfield (1995), Factors controlling joint spacing in interbedded sedimentary rocks: Integrating numerical models with field observations from the Monterey Formation, USA, in *Fractography: Fracture Topography as a Tool in Fracture Mechanics and Stress Analysis*, edited by M. S. Ameen, *Geol. Soc. London Spec. Publ., 92*, 215–233.

Gupta, A., and C. H. Scholz (2000), Brittle strain regime transition in the Afar depression: Implications for fault growth and seafloor spreading, *Geology, 28*(12), 1087–1090, doi:10.1130/0091-7613(2000)28<1087:BSRTIT>2.0.CO;2.

Guzman, C., E. Cristallini, and G. Bottesi (2007), Contemporary stress orientations in the Andean retroarc between 34°S and 39°S from borehole breakout analysis, *Tectonics, 26*, TC3016, doi:10.1029/2006TC001958.

Inbar, M., and C. Risso (2001), A morphological and morphometric analysis of a high density cinder cone volcanic field–Pyun Matru, south-central Andes, Argentina, *Z. Geomorph. N. F., 45*, 321–343.

Janza, F. J., , H. M. Blue, and J. E. Johnston (Eds.) (1975), *Manual of Remote Sensing: Theory, Instruments and Techniques*, vol. I, 867 pp., Am. Soc. of Photogramm. and Remote Sens., Bethesda, Md.

Kay, S. M., W. M. Burns, P. Copeland, and O. Mancilla (2006), Upper Cretaceous to Holocene magmatism and evidence for transient Miocene shallowing of the Andean subduction zone under the northern Neuquén Basin, in *Evolution of an Andean Margin: A Tectonic and Magmatic View from the Andes to the Neuquen Basin (35°–39°S lat)*, edited by S. M. Kay and V. A. Ramos, *Geol. Soc. Am. Spec. Pap., 407*, 19–60.

Kendrick, E., M. Bevis, R. Smalley Jr., B. Brooks, R. B. Vargas, E. Lauria, and L. P. Souto (2003), The Nazca-South America Euler vector and its rate of change, *J. S. Am. Earth Sci., 16*, 125–131, doi:10.1016/S0895-9811(03)00028-2.

Klotz, J., G. Khazaradze, D. Angermann, C. Reigber, R. Perdomo, and O. Cifuentes (2001), Earthquake cycle dominates contemporary crustal deformation in Central and Southern Andes, *Earth Planet. Sci. Lett., 193*, 437–446, doi:10.1016/S0012-821X(01)00532-5.

Legrand, D., A. Calahorrano, B. Guillier, L. Rivera, M. Ruiz, D. Villagomez, and H. Yepes (2002), Stress tensor analysis of the 1998–1999 tectonic swarm of northern Quito related to the volcanic swarm of Guaga Pichincha volcano, *Ecuador, Tectonophysics, 344*, 15–36, doi:10.1016/S0040-1951(01)00273-6.

Llambías, E. J. (1966), Geología y petrografía del volcán Payún Matrú, *Acta Geol. Lilloana, 8*, 265–310.

Luguet, A., D. G. Pearson, G. M. Nowell, S. T. Dreher, J. A. Coggon, Z. V. Spetsius, and S. W. Parman (2008), Enriched Pt-Re-Os isotope systematics in plume lavas explained by metasomatic sulfides, *Science, 319*, 453–456, doi:10.1126/science.1149868.

Mandelbrot, B. B. (1982), *The Fractal Geometry of Nature*, 468 pp., W. H. Freeman, New York.

Marchetti, D. W., T. E. Cerling, E. B. Evenson, J. C. Gosse, and O. Martinez (2006), Cosmogenic exposure ages of lava flows that temporarily dammed the Rio Grande and Rio Salado, Mendoza Province, Argentina, paper presented at Backbone of the Americas, Patagonia to Alaska Meeting, Geol. Soc. of Am., Mendoza, Argentina.

Mazzarini, F. (2004), Volcanic vent self-similar clustering and crustal thickness in the northern Main Ethiopian Rift, *Geophys. Res. Lett., 31*, L04604, doi:10.1029/2003GL018574.

Mazzarini, F. (2007), Vent distribution and crustal thickness in stretched continental crust: The case of the Afar Depression (Ethiopia), *Geosphere, 3*, 152–162, doi:10.1130/GES00070.1.

Mazzarini, F., and M. D'Orazio (2003), Spatial distribution of cones and satellite-detected lineaments in the Pali Aike Volcanic Field (southernmost Patagonia): Insights into the tectonic setting of a Neogene rift system, *J. Volcanol. Geotherm. Res., 125*, 291–305, doi:10.1016/S0377-0273(03)00120-3.

Mazzarini, F., G. Corti, P. Manetti, and F. Innocenti (2004), Strain rate bimodal volcanism in the continental rift: Debre Zeyt volcanic field, northern MER, *Ethiopia, J. Afr. Earth Sci., 39*, 415–420, doi:10.1016/j.jafrearsci.2004.07.025.

Meibom, A. (2008), The rise and fall of a great idea, *Science, 319*, 418–419, doi:10.1126/science.1153710.

Melchor, R., and S. Casadío (1999), Hoja Geológica 3766-III La Reforma, provincia de La Pampa, *Bol. 295*, 63 pp., Geol. Surv. of Argent., Buenos Aires.

Melnick, D., F. Charlet, H. P. Echtler, and M. De Batist (2006), Incipient axial collapse of the Main Cordillera and strain partitioning gradient between the central and Patagonian Andes Lago Laja, Chile, *Tectonics, 25*, TC5004, doi:10.1029/2005TC001918.

Mosquera, A., and V. A. Ramos (2006), Intraplate deformation in the Neuquén Embayment, in: *Evolution of an Andean Margin: A Tectonic and Magmatic View from the Andes to the Neuquen Basin (35°–39°S lat)*, edited by S. M. Kay and V. A. Ramos, *Geol. Soc. of Am. Spec. Pap., 407*, 97–123.

Musumeci, G., F. Mazzarini, G. Corti, M. Barsella, and D. Montanari (2005), Magma emplacement in a thrust ramp anticline: The Gavorrano Granite (northern Apennines, Italy), *Tectonics, 24*, TC6009, doi:10.1029/2005TC001801.

Nakamura, K. (1977), Volcanoes as possible indicators of tectonic stress, *J. Volcanol. Geotherm. Res., 2*, 1–16, doi:10.1016/0377-0273(77)90012-9.

Núñez, E. (1976), Descripción geológica de la Hoja 31e, Chical-Cò, Provincias de Mendoza y La Pampa, *Geol. Surv. of Argent.*, Buenos Aires.

Ouillon, G., C. Castaing, and D. Sornette (1996), Hierarchical geometry of faulting, *J. Geophys. Res., 101*, 5477–5487, doi:10.1029/95JB02242.

Pacheco, J. F., C. H. Scholz, and L. R. Sikes (1992), Change in the frequency-size relationship from small to large earthquakes, *Nature, 355*, 71–73, doi:10.1038/355071a0.

Pasquarè, G., A. Bistacchi, and A. Mottana (2005), Gigantic individual lava flows in the Andean foothills near Malargue (Mendoza, Argentina), *Rend. Fis. Acc. Lincei, 16*, 127–135, doi:10.1007/BF02904761.

Pasquarè, G., A. Bistacchi L. Francalanci, G. W. Bertotto, E. Boari, M. Massironi, and A. Rossotti (2008), Very long pahoehoe inflated basaltic lava *flows in the Payenia* Volcanic Province (Mendoza and La Pampa, Argentina), *Rev. Assoc. Geol. Argent.*, in press.

Petford, N., A. R. Cruden, K. J. W. McCaffrey, and J. L. Vigneresse (2000), Granite magma formation, transport and

emplacement in the Earth's crust, *Nature*, *408*, 669–673, doi:10.1038/35047000.

Polansky, J. (1954), Rasgos geomorfológicos de la provincia de Mendoza, in *Cuadernos de Investigaciones y Estudios*, vol. *4*, pp. 4–10, Minist. de Econ., Inst. de Invest. Econ. y Tecnol., Mendoza, Argentina.

Ramos, V. A. (1999), Plate tectonic setting of the Andean Cordillera, *Episodes*, *22*(3), 183–190.

Ramos, V. A., and S. M. Kay (2006), Overview of the tectonic evolution of the southern Central Andes of Mendoza and Neuquen (35°–39°S latitude), in *Evolution of an Andean Margin: A Tectonic and Magmatic View from the Andes to the Neuquen Basin (35°-39°S lat)*, edited by S. M. Kay and V. A. Ramos, *Geol. Soc. of Am. Spec. Pap.*, *407*, 1–17.

Renshaw, C. E. (1999), Connectivity of joints networks with power-law length distributions, *Water Resour. Res.*, *35*, 2661–2670, doi:10.1029/1999WR900170.

Risso, C., K. Németh, A. M. Combina, F. Nullo, and M. Drosina (2008), The role of phreatomagmatism in a Plio-Pleistocene high-density scoria cone field: Lancanelo Volcanic Field (Mendoza), Argentina, *J. Volcanol. Geotherm. Res.*, *169*, 61–86, doi:10.1016/j.jvolgeores.2007.08.007.

Roberts, S., D. J. Sanderson, and P. Gumiel (1999), Fractal analysis and percolation properties of veins, in *Fractures, Fluid Flow and Mineralization*, edited by K. J. W. McCaffrey, L. Lonergan, and J. J. Wilkinson, *Geol. Soc. London Spec. Publ.*, *155*, 7–16.

Rosenau, M., D. Melnick, and H. Echtler (2006), Kinematic constraints on intra-arc shear and strain partitioning in the southern Andes between 38° and 42°S latitude, *Tectonics*, *25*, TC4013, doi:10.1029/2005TC001943.

Rubin, A. M. (1993), Dikes vs. diapirs in viscoelastic rock, *Earth Planet. Sci. Lett.*, *119*, 641–659, doi:10.1016/0012-821X(93)90069-L.

Scholz, C. H. (2002), *The Mechanics of Earthquakes and Faulting*, 2nd ed., Cambridge Univ. Press, New York.

Somoza, R. (1998), Updated Nazca (Farallon)–South America relative motions during the last 40 My: Implications for mountain building in the central Andean region, *J. S. Am. Earth Sci.*, *11*, 211–215, doi:10.1016/S0895-9811(98)00012-1.

Spyropoulos, C., C. H. Scholz, and B. E. Shaw (2002), Transition regimes for growing crack populations, *Phys. Rev. E*, *65*, 056105, doi:10.1103/PhysRevE.65.056105.

Stauffer, D., and A. Aharony (1992), *Introduction in Percolation Theory*, 2nd ed., 190 pp., Taylor and Francis, Philadelphia, Pa.

Tassara, A., H.-J. Götze, S. Schmidt, and R. Hackney (2006), Three-dimensional density model of the Nazca plate and the Andean continental margin, *J. Geophys. Res.*, *111*, B09404, doi:10.1029/2005JB003976.

Tibaldi, A. (1995), Morphology of pyroclastic cones and tectonics, *J. Geophys. Res.*, *100*, 24,521–24,535, doi:10.1029/95JB02250.

Tibaldi, A. (2005), Volcanism in compressional tectonic settings: It is possible?, *Geophys. Res. Lett.*, *32*, L06309, doi:10.1029/2004GL021798.

van Wyk de Vries, B., S. Self, P. W. Francis, and L. Keszthelyi (2001), A gravitational spreading origin for the Socompa debris avalanche, *J. Volcanol. Geotherm. Res.*, *105*, 225–247, doi:10.1016/S0377-0273(00)00252-3.

Vrabel, J. (1996), Multispectral imagery band sharpening study, *Photogramm. Eng. Remote Sens.*, *62*, 1075–1083.

Walsh, J. J., and J. Watterson (1993), Fractal analysis of fracture pattern using the standard box-counting technique: Valid and invalid methodologies, *J. Struct. Geol.*, *15*, 1509–1512, doi:10.1016/0191-8141(93)90010-8.

Wang, K., Y. Hu, M. Bevis, E. Kendrick, R. Smalley Jr., R. B. Vargas, and E. Lauria (2007), Crustal motion in the zone of the 1960 Chile earthquake: Detailing earthquake-cycle deformation and forearc-sliver translation, *Geochem. Geophys. Geosyst.*, *8*, Q10010, doi:10.1029/2007GC001721.

Watanabe, T., T. Koyaguchi, and T. Seno (1999), Tectonic stress controls on ascent and emplacement of magmas, *J. Volcanol. Geotherm. Res.*, *91*, 65–78, doi:10.1016/S0377-0273(99)00054-2.

Wise, D. U., R. Funicello, M. Parotto, and F. Salvini (1985), Topographic lineament swarms: Clues to their origin from domain analysis of Italy, *Geol. Soc. Am. Bull.*, *96*, 952–967, doi:10.1130/0016-7606(1985)96<952:TLSCTT>2.0.CO;2.

Wu, H., and D. D. Pollard (1995), An experimental study of the relationships between joint spacing and layer thickness, *J. Struct. Geol.*, *17*, 887–905, doi:10.1016/0191-8141(94)00099-L.

Zakir, F. A., M. H. T. Quari, and M. E. Mostafa (1999), New optimizing technique for preparing lineament density maps, *Int. J. Remote Sens.*, *20*, 1073–1085, doi:10.1080/014311699212858.